Nanoscale

PAPER

View Article Online
View Journal | View Issue

Cite this: *Nanoscale*, 2025, **17**, 17146

Electrospun natural product-based Shidu Formula for the management of psoriasis†

Ruodan Xu, *[a] Mengyuan Zhou, [b] Yi Tang,[b] Can Cao, [a] Yanxin Jiang,[a] Jing Li,[b] Chen Wang,[a] Xi Wu,[c] Ping Song[d] and Ning Li*[a]

The Shidu Formula (SDF) ointment is a natural product-based medicine that has a long history of use in treating psoriasis. Compared to standard first-line clinical medications, SDF remedies present certain advantages, particularly in terms of causing minimal skin irritations. However, several challenges have limited their widespread applications. These include the sticky nature of SDF ointments, which can hinder drug penetration and lead to staining of the skin and clothing, and delayed onset of effects that often necessitates higher dosages. Therefore, the development of innovative topical solutions is highly required to deliver the complex components of SDF effectively. In this study, we developed an amphiphilic blended membrane of polycaprolactone (PCL) and polyethylene oxide (PEO) using electrospinning, successfully transforming the SDF ointment into nanofibrous meshes. We confirmed that it was feasible to incorporate a maximum of 5% SDF through morphological, physiological, and pharmacological assessment. The release profile of the principal active components verified that berberine chloride and gallnut were released in bursts. *In vivo* experiments further demonstrated the benefits and biocompatibility of the SDF–PCL/PEO membrane in the management of IMQ-induced psoriasis-like skin inflammation, as demonstrated by severity index scoring and pathological evaluations. Notably, converting the ointment into nanofibrous meshes addressed the typical challenges associated with conventional SDF ointment, resulting in significantly improved efficacy, short application times, controllable dosages, and reduced staining of the skin and clothes. This work provides a promising approach for transforming complex natural products into effective external treatment options for psoriasis.

Received 8th May 2025,
Accepted 18th June 2025

DOI: 10.1039/d5nr01873k

rsc.li/nanoscale

Introduction

Psoriasis is a chronic, immune-mediated skin disease characterized by thick, scaly, itchy, and erythematous plaques, which can significantly impact patients' quality of life.[1,2] While current treatments for psoriasis, such as topical corticosteroids, vitamin D analogues, and biologics, can effectively alleviate symptoms, they often fail to provide sustained results and may lead to adverse side effects.[3–5] In recent years, natural product-based medicine has gained global recognition as a viable option for managing psoriasis.[6,7] By emphasizing the reduction of adverse side effects, promoting sustainable long-term solutions, and addressing underlying causes rather than just relieving symptoms, natural products present compelling alternatives to prevailing conventional therapies.

Shidu Formula (SDF) is a traditional Chinese medicine that consists of the original composition of crude extracts from five plants and minerals: *Phellodendron chinense*, *Indigo naturalis*, *Gallae chinensis*, Gypsum fibrosum, and calamine. The ointment formulation of SDF offers several distinct clinical advantages over conventional topical therapies, such as corticosteroids or vitamin D analogues, by minimizing skin atrophy and irritation while maintaining comparable anti-psoriatic effects.[8] The benefits of SDF are attributed to its multicomponent formulations, which can achieve a synergistic effect, leading to a better overall result than single-agent therapies in psoriasis. Pharmacological studies have identified several essential bioactive compounds in SDF, such as berberine chloride from *Phellodendron chinense*, gallic acid from *Gallae chinensis*, indirubin, indigo and tryptanthrin from *Indigo naturalis*.[9–11] In particular, berberine chloride and gallic acid are known to address immune dysregulation and keratinocyte hyperproliferation.[9,10,12] The three major components of

[a]*Department of Biomedical Engineering and Technology, Institute of Basic Theory for Chinese Medicine, China Academy of Chinese Medical Sciences, Beijing, 100700, China. E-mail: ruodanxu@gmail.com, lili.li.ning@gmail.com*
[b]*Department of Nephropathy, Dong Zhi Men Hospital, Beijing University of Chinese Medicine, Beijing, PR China*
[c]*Department of Gastroenterology, Beijing Hospital, National Center of Gerontology, Institute of Geriatric Medicine, Chinese Academy of Medical Sciences, PR China*
[d]*Xiyuan Hospital, China Academy of Chinese Medical Sciences, Beijing, 100091, China*

† Electronic supplementary information (ESI) available. See DOI: https://doi.org/10.1039/d5nr01873k

Indigo naturalis have been demonstrated to play a significant role in the pathogenesis of psoriasis.[11,13] Despite its promising clinical applications, SDF faces challenges associated with percutaneous absorption due to the hydrophobic properties of its constituents and the ointment formulation.[14–18] Besides, plant-based topical ointments often encounter three common difficulties.[19,20] First, these ointments feature greasy and dark brown semi-solid ingredients that can leave undesirable residues on both skin and clothing. Second, the airtight property of the formulation may cause clogged pores and increase the risk of bacterial growth. Third, the preservation of the ointment is susceptible to oxidation, deterioration, contamination, and instability. Additionally, the unpredictable dosage of SDF ointment frequently results in inconsistent therapeutic outcomes and poor patient compliance, which can lead to its discontinuation in practical use. To address these challenges for the treatment of psoriasis, it is primarily essential to develop innovative dosage forms and enhance the transdermal bioavailability of SDF.

Electrospinning technology has emerged as an effective method for addressing challenges in topical drug delivery by creating robust three-dimensional structures that yield amorphous or crystalline solid dispersions.[21,22] The impressive mechanical properties of nanofibers, along with their high surface area-to-volume ratio, notable porosity, and flexibility, make them excellent candidates for developing topical delivery systems for traditional Chinese medicine.[23–25] The dissolvability of drugs is a crucial factor influencing the bioavailability of Chinese medicine, which often suffers from low solubility due to its lipophilic nature.[22] This challenge can be mitigated by integrating Chinese medicine into nanofibers composed of water- or organic-soluble polymers, thereby significantly enhancing the dissolution rate. Another notable advantage of nanofibers is their customizable properties. By adjusting production parameters, one can achieve precise control over characteristics such as polarity, fiber diameter, porosity, and mat thickness to meet specific delivery requirements. Additionally, nanofibers allow for a high loading capacity and can be engineered for controlled drug release profiles, which can be adapted using various loading methods, including co-electrospinning, surface immobilization, and co-axial techniques. These features enable efficient drug loading while promoting amorphous dispersion, ultimately improving solubility and enhancing transdermal permeability. Moreover, the superior air permeability of electrospun nanofiber membranes effectively addresses the three challenges associated with topical ointments.

To fulfill the requirements for effective skin drug delivery, polycaprolactone (PCL) and polyethylene oxide (PEO) have been employed as the nanofiber matrix due to their biocompatibility, controlled drug release capabilities, mechanical properties, and amphiphilic nature. PCL, a synthetic polymer approved by the Food and Drug Administration (FDA), is recognized for its biocompatibility and controlled degradation kinetics, which are essential for sustained drug release applications.[26,27] Meanwhile, PEO enhances the overall biocompatibility of the formulation, minimizing the risk of adverse reactions in biological environments.[28–30] The hydrophobic nature of PCL facilitates the gradual release of drugs over an extended period, while the hydrophilic PEO contributes to an initial burst release, creating an optimal balance between immediate and sustained drug release. Furthermore, PCL's mechanical strength and structural stability are vital for maintaining the integrity of the patch during the topical application, whereas PEO adds flexibility and elasticity to the nanofibers, enhancing patient comfort.[31] The hydrophilic properties of PEO also promote moisture retention, an important aspect in the treatment of psoriasis. This not only improves drug release but also enhances the adhesion of the patch to the skin. Compared to other systems, such as poly(lactic-*co*-glycolic acid) (PLGA), which exhibit higher hydrophobicity, or polyvinyl alcohol (PVA), known for its high hydrophilicity but poorer long-term stability, the PCL/PEO blend provides an optimal balance of hydrophilicity and mechanical stability that neither PLGA nor PVA can achieve independently. A 5% PCL/PEO (80 : 20, v/v) formulation was selected for developing the skin drug delivery system, notable for its uniform fiber diameters with a distribution range of 0.73 ± 0.19 μm, which serves as an effective delivery vehicle for *Indigo naturalis*, facilitating a more favorable release profile for the compounds indirubin and tryptanthrin.[32]

In the current study, we managed the challenges associated with ointment formulations of SDF by selecting PCL/PEO as the blending material for the electrospinning process. The evaluations of both *in vitro* characterization and drug release, as well as *in vivo* efficacy assessments, demonstrated the feasibility of these nanofiber materials as effective drug delivery systems for SDF in the treatment of IMQ-induced psoriasis-like skin inflammation. Notably, the successful incorporation of a multi-component SDF formula with the simple PCL/PEO vehicle offers a broadly applicable strategy for innovative topical ointment formulations.

Materials and methods

Materials

Indigo naturalis was obtained from Beijing HuaMiao Pharmaceutical Co., Ltd (Beijing, China). *Phellodendron chinense*, *Gallae chinensis*, calamine, and Gypsum fibrosum were sourced from Yinchuan Baopu Internet Hospital Co., Ltd (Ningxia, China). The reference standards of indigo (98.8% purity), indirubin (98.9% purity), berberine chloride (91% purity), and gallic acid (90.8% purity) were purchased from the National Institutes for Food and Drug Control (Beijing, China). PCL of 80 kDa (in number M_n) and PEO (M_v = 300 kDa) were obtained from Sigma-Aldrich (St Louis, MO, USA). 1,1,1,3,3,3-Hexafluoro-2-propanol (HFIP) was supplied by Aladdin Biochemical Technology (Shanghai, China). Methanol and acetonitrile (HPLC grade) were purchased from Thermo Fisher Scientific (Fair Lawn, NJ, USA).

Electrospinning

PCL and PEO were dissolved in HFIP at a ratio of 8 : 2 (v/v) and stirred overnight to achieve a homogeneous solution. A formulation of SDF was prepared by mixing *Indigo naturalis*, *Phellodendron chinense*, *Gallae chinensis*, Gypsum fibrosum, and calamine at a ratio of 15 : 31 : 31 : 18 : 9 (w/w). The SDF at a concentration of 0.2%, 1%, and 5% (w/v) was gradually added to the PCL/PEO mixture while continuously mixing, respectively. The resulting solutions were transferred to a 5 mL syringe, which was then mounted on a syringe pump in an electrospinning machine (ET-2535DC, Ucalery, Beijing, China). A positive high voltage was connected to a needle using an alligator clip, while the collecting plate, covered with aluminum foil, was grounded. The process parameters were set at a voltage of 7 kV, a flow rate of 0.15 mm min^{-1}, and a distance from the needle tip to the collector of 13 cm. The temperature in the environment was maintained at 32 °C, with humidity levels ranging from 30% to 40%. The fabricated nanofibrous membranes were frozen overnight and then freeze-dried using a freeze-drying system (LGJ-10C, Foring Technology, Beijing, China).

Scanning electron microscopy (SEM) and surface evaluation

The nanofibrous membranes were sputter-coated with a thin layer of gold before their examination. The surface of the samples was observed using field emission scanning electron microscopy and energy dispersive X-ray spectrometry (EDS; Phenom Pharos G2, Eindhoven, Netherlands) at an accelerating voltage of 10 kV. The diameters of the resulting fibers were measured at 100 random locations on each fiber, and the average diameter was calculated using image analysis software (ImageJ, NIH, USA). The elemental composition and distribution were obtained by EDS.

Fourier transform infrared spectroscopy (FTIR)

The chemical bonds of indigo, indirubin, berberine chloride and gallic acid, along with those in PCL/PEO and SD-PCL/PEO nanofibers, were analyzed using an IRXross FTIR spectrometer (SHIMADZU, Kyoto, Japan) in transmission mode at room temperature. The infrared spectra were recorded in the range of 4000 to 400 cm^{-1}, with a resolution of 4 cm^{-1}. Baseline and atmospheric corrections were applied to each spectrum to minimize background interference and enhance signal accuracy before further data analysis.

Water contact angle

The contact angles of the nanofibrous membranes were measured using a surface tension meter (Theta Flow, Biolin Scientific, Espoo, Finland). A droplet of 5 μL of deionized distilled water (ddH_2O) was used, and the water contact angle was recorded over a period of 10 s. The measurement was performed three times, and the average value was calculated.

Mechanical properties

The mechanical properties of the nanofibers were assessed using an electric universal testing machine (EZ Test, Shimadzu Corporation, Japan) equipped with a 10 N load cell. For each group, the membranes were cut into rectangular pieces with uniform dimensions of 1 by 10 cm. Tensile testing of the nanofiber membranes was conducted at a speed of 10 mm min^{-1}. Young's modulus (E) is derived from the slope of the linear segment of the stress–strain curve. Stress (σ) is defined as the force (F) applied to a fiber divided by its cross-sectional area (A). Strain (ε) is calculated by dividing the change in length (ΔL) by the original length (L_0) of the fiber. The Young's modulus is typically calculated by averaging the results of multiple tests to enhance precision and reliability in the measurements. All experiments were carried out in triplicate.

$$E = \sigma/\varepsilon$$

High-performance liquid chromatography (HPLC)

The contents of indigo, indirubin, berberine chloride, and gallic acid in the samples were determined by HPLC (Waters Corporation, Singapore), respectively. For the chromatographic analysis of indigo and indirubin, a C18 column was employed as the stationary phase (Agilent, Stable Bond 300, 250 mm × 4.6 mm, 5 μm). The mobile phase consisted of a mixture of methanol and deionized water (ddH_2O) in a ratio of 60 : 40 (v/v), with a flow rate maintained at 1 mL min^{-1}. The retention times for indigo and indirubin were recorded at 6 min and 9.5 min, respectively. The HPLC detection of berberine chloride was conducted on a ZORBAX 300 C18 column (Agilent, Stable Bond, 250 mm × 4.6 mm, 5 μm) utilizing a gradient program. The gradient mobile phase system comprised solvent A, which contained 0.1% (v/v) phosphoric acid with 0.2% sodium dodecyl sulfonate (SDS) in water, and solvent B, which was acetonitrile. The separation was executed following a gradient program established as follows: an initial composition of 30% v/v B at zero time; increasing to 50% v/v B from 12 to 15 min; holding 50% v/v B from 16 to 24 min; ramping up to 90% v/v B from 25 to 28 min; holding 90% v/v B from 29 to 35 min. Following a 7 min run, the gradient program returned to its initial conditions, and the analytical column was reconditioned for 3 min. The flow rate remained constant at 1.0 mL min^{-1} throughout the analysis, with an injection volume of 10 μL. The detection wavelength was initially set at 284 nm, subsequently adjusted at designated time intervals to 265 nm, and finally returned to 284 nm. For the analysis of gallic acid, a C18-A column was utilized as the stationary phase (Agilent, Polaris 5, 250 mm × 4.6 mm, 5 μm), with a mobile phase composed of methanol and 0.1% phosphoric acid water (5 : 95, v/v), at a flow rate of 1 mL min^{-1} with the retention time being 10.2 min. The quantities of indigo, indirubin, berberine chloride, and gallic acid were quantified at 606 nm, 292 nm, 284 nm, and 273 nm, respectively.

In vitro drug release

A release study was conducted to determine the release profiles of indigo, indirubin, berberine chloride, and gallic acid from SDF–PCL/PEO (30 mg) in a 3 mL solution of 50% methanol (pH 5.5) at 34 °C, with continuous stirring at 200 rpm.

Over a period of 24 h, 1 mL volumes of solution were collected from each sample at intervals of 10, 20, 30, 40, 50, and 60 min, as well as at 2, 4, 8, 12, and 24 h. To maintain a constant volume of 3 mL, 1 mL of fresh solution was added to each sample after each collection. The collected samples were filtered through a 0.45 μm filter and analyzed by HPLC to quantify the amount of released drug. All measurements were performed in triplicate.

Animal model and treatment

Male BALB/c mice (6–8 weeks, weighing 20 ± 2 g) were purchased from Beijing Vital River Laboratory Animal Technology Co., Ltd (Beijing, China). Throughout the experimental period, all animals were group-housed with unrestricted access to food and water in a controlled environment maintained at a constant temperature and a standard light/dark cycle. The animal studies adhered to the National Guidelines for the Care of Laboratory Animals and were performed in accordance with institutional regulations, having received approval for the experimental protocols from the Institutional Animal Care and Use Committee at the Institute of Basic Theory for Chinese Medicine, China Academy of Chinese Medical Sciences (No. IBTCMCACMS21-2303-02, Date: April 22, 2023).

Imiquimod (IMQ), a potent immune activator and ligand for TLR7/8, was utilized for the development of a psoriasis-like mouse model through topical application. The mice were assigned to eight groups, with all groups except the control group receiving IMQ treatment. IMQ (62.5 mg of 5% IMQ cream Aldara®, 3M Pharmaceuticals, St Paul, MN) was administered daily to the shaved backs of area 3 cm × 2 cm and 5 mg of IMQ to the right ears of area 1 cm × 1 cm every 24 h for 7 consecutive days to induce psoriasis-like lesions.[33,34] In addition to the control group (without IMQ treatment) and the model group (IMQ treatment only), the inflamed skin areas of the other six groups were also treated daily with clobetasol propionate (CP), SDF ointment, PCL/PEO, 0.2% SDF–PCL/PEO, 1% SDF–PCL/PEO, and 5% SDF–PCL/PEO, respectively. Following the treatment, the fiber membranes were applied topically to the dorsal surface of the mice (3 cm × 2 cm) and the right ear (1 cm × 1 cm) with drops of water and were left *in situ* for 30 min. Body weight and images of skin lesions were recorded every day. On the eighth day, the mice were sacrificed, and skin samples from the back were collected for pathological examination.

Evaluation of the severity of psoriatic skin lesion

An objective scoring system based on the clinical psoriasis area and severity index (PASI) was employed to assess the severity of inflammation on the dorsal skin of mice.[35] Erythema and scaling scores were recorded daily through a blind evaluation using a scale from 0 to 4 (0 – none; 1 – slight; 2 – moderate; 3 – marked; and 4 – very marked). The scores for scaling and erythema were summed to obtain a total score ranging from 0 to 8. Measurements were taken once daily for seven consecutive days following treatment administration.

Hematoxylin and eosin (H&E) staining

At the end of the experiments, the skin, liver, kidneys, and spleen from mice were fixed in 4% paraformaldehyde for 48 h, embedded in paraffin, and subsequently sectioned into 4 μm slices using a microtome (Leica, Nussloch, Germany). Following deparaffinization and rehydration, the tissue sections were stained with hematoxylin–eosin staining solution (Solarbio), according to the manufacturer's protocol. All images were captured using the ScanScope slide scanner (Aperio, CA, USA) along with an image analysis system (Aperio V.10.2).

Immunohistochemistry (IHC)

For IHC staining, hydrated sections were subjected to antigen retrieval using a citrate solution (Beyotime, Shanghai, China) at 95 °C for 15 min, followed by cooling down to room temperature (RT). To block non-specific binding sites, 5% goat serum in PBS was utilized after inactivating endogenous peroxidase. Primary antibodies, including anti-Ki67 (ab16667, 1 : 400), anti-CD68 (ab125212, 1 : 2000), and anti-CD31 (ab124432, 1 : 1000) from Abcam, were applied overnight for staining at 4 °C. The sections were then incubated with a secondary antibody, goat anti-rabbit IgG (Zhongshan Golgen Bridge Biotechnology, Beijing, China), for 30 min at RT. Finally, the sections were stained with fresh diaminobenzidine (Zhongshan Golgen Bridge Biotechnology) and counterstained with hematoxylin. All images were captured using the ScanScope slide scanner with Aperio ImageScope analysis software.

Tissue optical clearing

The lesioned skin tissues were collected and immersed in 4% paraformaldehyde (PFA) in PBS (pH 7.4). The fixed skin samples were then further processed by immersing in 4% PFA at 4 °C overnight, followed by washing with PBS twice for two hours each at room temperature (RT). For tissue clearing and immunostaining, the samples underwent a clearing process using a tissue clearing kit (Nuohai Life Science, Co., Ltd, Shanghai, China). Delipidation was conducted by immersing each sample in a mixture of solution A and solution B for one day at 37 °C. After delipidation, the samples were washed three times in PBS for two hours each at 4 °C. The cleared samples were then subjected to immunostaining by incubating them in KRT-7 (1 : 400, Abcam, Cambridge, MA, USA), CD31 (1 : 1000, Abcam), and DAPI for two days at 4 °C with shaking at 60 rpm, followed by three washes in PBS for three hours at RT. Reactive index matching was achieved by treating the immunostained samples with solution C and shaking them at 25 °C for two days. For gel embedding, a 2 mm deep gel solution was added to a customized cuvette and cooled at 4 °C for 30 min to semi-solidify. The samples were gently placed into the cuvette, submerged in the gel solution, and subsequently cooled at 4 °C for two hours before imaging.

3D imaging with light-sheet fluorescence microscopy

Following tissue optical clearing, 3D imaging was conducted using a Nuohai LS-18 light-sheet fluorescence microscope

(Nuohai Life Science). A 6.3× objective (6 tiles, imaging resolution: x = 2 μm, y = 2 μm, z = 5 μm) was selected for image acquisition. The raw imaging data were then processed for image reconstruction, and the resulting images were further processed and optimized using Imaris (v. 9.0, Bitplane, Oxford, UK) and Amira image processing software. All images underwent background subtraction, and contrast was uniformly enhanced for clarity.

Statistical analysis

Data are represented as mean value ± the standard error of the mean (SEM) and were analyzed with a one-way analysis of variance (ANOVA), followed by the Bonferroni *post hoc* test. Significance was determined at $p < 0.05$. All statistical analyses and figure generation were performed using Prism 9 (GraphPad, San Diego, CA, USA) or OriginPro (OriginLab Corporation, Northampton, MA, USA).

Results and discussion

Preparation and characterization of electrospun SDF–PCL/PEO nanofibrous membranes

To improve the bioavailability of SDF for the topical treatment of IMQ-induced psoriasis-like skin inflammation, PCL/PEO copolymers were developed as a transdermal drug delivery system through electrospinning. The optimal composition of 5% PCL/PEO was identified with an 80 : 20 (w/w) ratio.[32] Various SDF concentrations (0.2%, 1%, 5%) were incorporated by producing morphologically smooth, bead-free, and randomly oriented nanofibers (Fig. 1A–D). Following this methodology, the average diameter of the PCL/PEO nanofibers was measured at 0.72 ± 0.01 μm (Fig. 1A and A′). The subsequent incorporation of SDF, increasing from 0.2% to 5%, resulted in a modest increase in fiber size, with measurements of 0.75 ± 0.07 μm for 0.2% SDF–PCL/PEO (Fig. 1B and B′), 0.76 ±

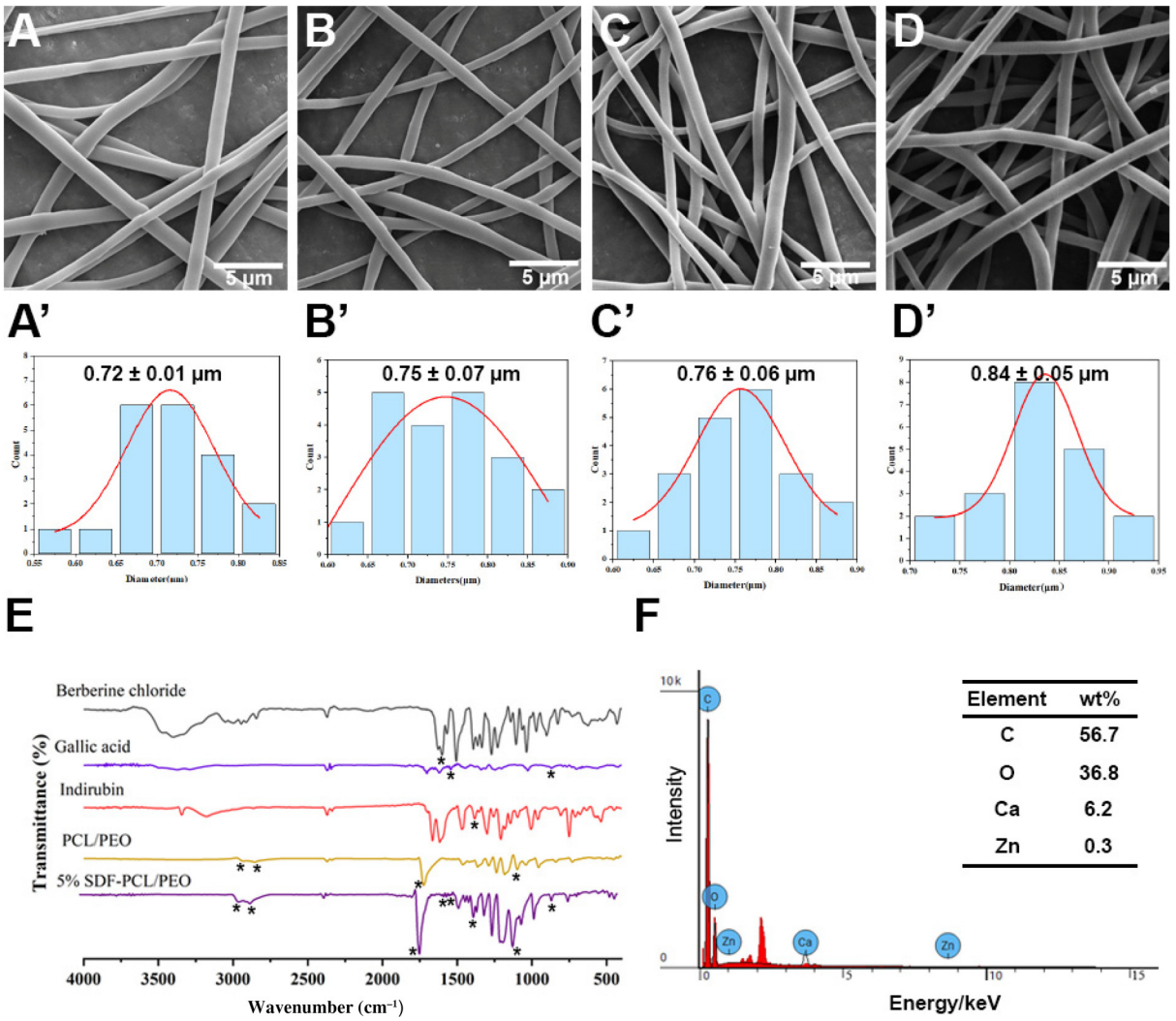

Fig. 1 Characterization of the nanofibrous meshes. (A–D) SEM images of PCL/PEO (A), 0.2% SDF–PCL/PEO (B), 1% SDF–PCL/PEO (C), and 5% SDF–PCL/PEO (D). Scale bar: 5 μm as indicated. (A′–D′) Fiber diameter distributions of the four groups of meshes corresponding to A–D. (E) FTIR spectra of berberine chloride, gallic acid, indirubin, PCL/PEO, and SDF–PCL/PEO. The asterisks (*) indicate the characteristic peaks of the samples listed in Table S1.† (F) EDS analysis of the SDF–PCL/PEO nanofibrous membrane.

0.06 μm for 1% SDF–PCL/PEO (Fig. 1C and C′), and 0.84 ± 0.05 μm for 5% SDF–PCL/PEO (Fig. 1D and D′). To confirm the successful incorporation of SDF into the PCL/PEO nanofibrous mesh, the three main active ingredients of SDF, namely indirubin, berberine chloride, and gallic acid, were analyzed using FTIR (Fig. 1E). The FTIR spectra provide insights into the molecular structure and chemical distinctions, which can be used to identify chemical compositions and alterations. The typical spectra of PCL and PEO were detected in both the PCL/PEO and SDF–PCL/PEO membranes. Absorption peaks at 2940 cm^{-1} and 2863 cm^{-1} corresponded to O–H stretching, while a strong absorption peak at 1726 cm^{-1} indicated a symmetric stretching vibration of C═O, which is exclusive to PCL. The symmetric stretching vibration of C–O–C was revealed by a characteristic peak at 1103 cm^{-1} for PEO. To further elucidate these findings, individual FTIR spectra of indirubin, berberine chloride, and gallic acid were obtained. The lower signal plots of Fig. 1E illustrate that the spectra of SDF–PCL/PEO within the range of 850–1635 cm^{-1}, associated with the stretching vibrations of the conjugated system of C═N^+, C═O, and C–C groups, corresponded to all three tested molecules. A band recorded at 1635 cm^{-1} is believed to correspond to the iminium (C═N^+) double bond present in berberine chloride. Additionally, two peaks of gallic acid at around 1541 cm^{-1} (C–C bonds) and 872 cm^{-1} (aromatic group Ar–C stretching vibration) are present in SDF–PCL/PEO. A subtle band at 1360 cm^{-1} (aromatic amine C–N stretching vibration), associated with indirubin, was also verified in SDF–PCL/PEO. Calcium (Ca) is the primary chemical component of Gypsum fibrosum, while zinc (Zn) is the key element in calamine. To further investigate the incorporation of Gypsum fibrosum and calamine into the PCL/PEO membrane, energy dispersive X-ray spectroscopy (EDS) was performed to analyze the chemical composition of the SDF within the PCL/PEO membrane. The EDS analysis, as depicted in Fig. 1F, demonstrates the presence of Ca and Zn in the SDF–PCL/PEO membrane. The compositional analysis of the EDS spectrum reveals a weight ratio of C/O/Ca/Zn in the membrane of 56.7/36.8/6.2/0.3, indicating that the SDF–PCL/PEO membrane contains a small amount of Gypsum fibrosum and trace levels of calamine, which is also consistent with their mixing ratio. These findings confirm the successful encapsulation of SDF within PCL/PEO. Collectively, this data set validates the miscibility of SDF and its principal components with PCL/PEO during the formation of electrospun nanofibers.

Surface hydrophilicity of an SDF–PCL/PEO nanopatch

The electrospun SDF–PCL/PEO nanofibrous mesh is designed to function as a membrane that requires hydration prior to drug release and permeation through the skin barrier. To assess the surface wettability and hydrophilicity of the nanofibrous membrane, we performed contact angle measurements between water droplets and the membrane surface. A lower contact angle signifies a higher hydrophilicity of the tested membrane. It is well established that PEO, with hydrophilic functional groups in its structure, enhances the hydrophilicity when blended with a hydrophobic polymer PCL, leading to a noticeable reduction in the water contact angle. This was confirmed in the non-drug-loaded PCL/PEO composition at a ratio of 80 : 20 (w/w), as illustrated in Fig. 2A. Conversely, since SDF contains non-polar side groups, increasing the SDF content in the PCL/PEO membrane resulted in a higher water contact angle, indicating a progressive shift towards enhanced hydrophobicity of the SDF nanofibrous membrane. Thus, the incorporation of PEO effectively improved the wettability of PCL, which could also be further adjusted by varying the SDF content. This amphiphilic characteristic of SDF–PCL/PEO is indeed a desired attribute for topical drug application.

Mechanical properties

As a topical formulation, it is crucial for the mechanical properties of the nanofibrous mesh to mimic those of human skin, which notably is highly anisotropic and viscoelastic, with its Young's modulus ranging from 5 kPa to 140 MPa serving as an important metric for assessing the characteristics of the nanofibers.[36] On analyzing the stress and strain mechanical properties of the nanofibrous membranes (Fig. 2B and C), the PCL/PEO exhibited a Young's modulus of 0.336 ± 0.01 MPa, a tensile strength of 4.42 ± 0.1 MPa, and an elongation at break of 660.33 ± 15.11%. In comparison, the Young's modulus of the 0.2% SDF–PCL/PEO fibers demonstrated a decrease, along with a reduction in elongation at break. This change can likely be attributed to the drug loading altering the molecular rearrangement within the polymer network matrix, thereby potentially weakening its structure and reducing its ability to resist deformation under stress.[37,38] The incorporation of SDF into PCL/PEO led to a decrease in both tensile strength and elongation at break, which can be associated with the effects of SDF in its amorphous form on the intermolecular interactions within the PCL/PEO. When the SDF content increases to 5%, the Young's modulus of the SDF–PCL/PEO dropped to 0.066 ± 0.003 MPa, while the tensile strength and elongation at break decreased to 2.80 ± 0.014 MPa and 500.33 ± 12.28.0%, respectively. Overall, the SDF nanofibrous membranes demonstrated favorable flexibility and extensibility, making them promising candidates for dermal drug delivery applications.

In vitro drug release of the SDF–PCL/PEO nanofibrous membrane

To assess the therapeutic potential of SDF–PCL/PEO, we initially examined the dynamic release profiles of indirubin, berberine chloride, and gallic acid. As shown in Fig. 3A, approximately 54.4% of berberine chloride was released from PCL/PEO nanofibers within the first 30 min, gradually increasing to 71.7% after 1 h. In contrast, gallic acid demonstrated a more rapid profile, with around 93.6% released in the initial 30 min, eventually reaching 100% after an additional 30 min (Fig. 3B). However, no distinct characteristic peaks were observed for indirubin, which was most likely due to relatively low content of active components in the fibers. These results indicate a more efficient release of gallic acid compared to berberine chloride. Moreover, the significant initial burst release

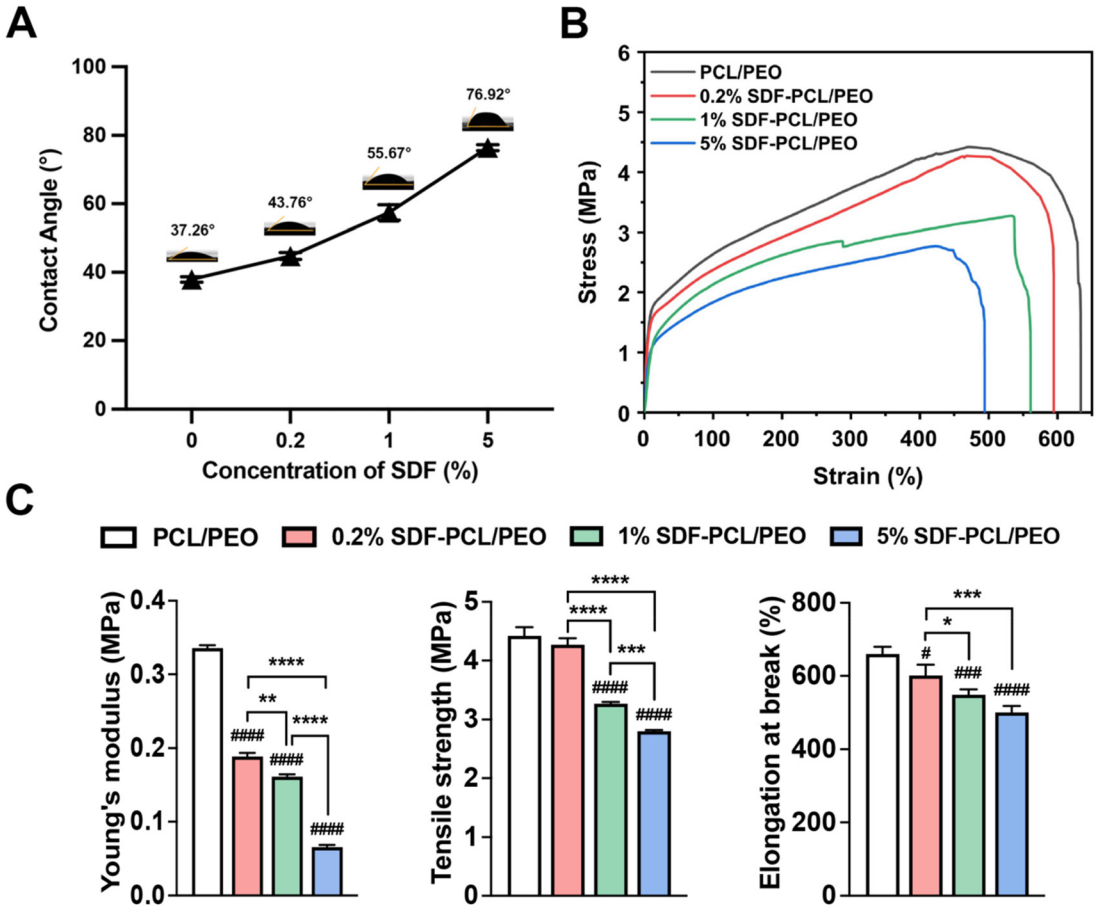

Fig. 2 Wettability and mechanical properties of nanofibrous meshes. (A) Water contact angle measurements of PCL/PEO nanofibrous meshes loaded with 0.2% SDF, 1% SDF or 5% SDF. (B) Stress–strain curves of the PCL/PEO, 0.2% SDF–PCL/PEO, 1% SDF–PCL/PEO, and 5% SDF–PCL/PEO nanofibrous meshes. (C) Young's modulus, tensile strength, and elongation at break of the four groups of nanofiber meshes. Data are presented as mean ± SEM. $^{\#}p < 0.05$, $^{\#\#\#}p < 0.005$, and $^{\#\#\#\#}p < 0.001$ compared to PCL/PEO; $^{*}p < 0.05$, $^{**}p < 0.01$, $^{***}p < 0.005$, and $^{****}p < 0.001$ between treatments as indicated.

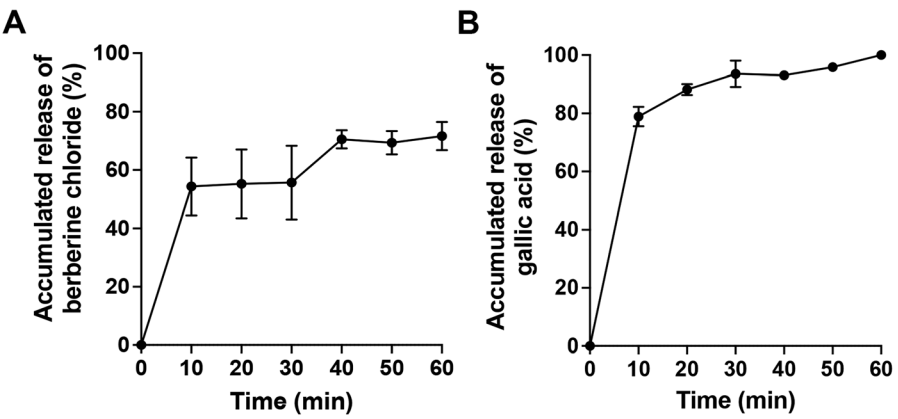

Fig. 3 Drug release profiles of SDF–PCL/PEO nanofiber meshes. (A) Cumulative drug release curve for berberine chloride from SDF–PCL/PEO nanofiber meshes. (B) Cumulative drug release curve for gallic acid from SDF–PCL/PEO nanofiber meshes. Bars represent the mean ± SEM of 3 independent assays.

of the SDF components, in relation to the release observed over 1 h, suggests that a short-term application of the nanofibrous membrane for just 30 min may be sufficient to meet therapeutic requirements.

The burst release of ingredients from SDF–PCL/PEO can be attributed to several factors related to the properties of the polymers and the structure of the nanofibers. First, PEO is a hydrophilic polymer, which means it readily absorbs water and swells. When incorporated into the nanofiber, PEO can quickly take up water from the surrounding environment, leading to the rapid dissolution and release of the drug located at or near the surface of the fibers. This swift water absorption and swelling can result in a significant amount of the drug being released in a short time frame, thus causing the burst release phenomenon. Second, the solubility of the drug in the release medium is crucial. Hydrophilic drugs, which exhibit higher solubility in water, will dissolve and be released from the nanofibers more rapidly. Additionally, the interaction between PCL (a hydrophobic polymer) and PEO influences drug release. PEO has the capability of forming channels or pathways within the nanofiber matrix, facilitating the rapid diffusion of the drug. Lastly, the initial burst release is often due to the quick diffusion of the drugs, which are deposited on the surface of the nanofibers. These surface-bound drugs are more readily accessible to the release medium, resulting in faster dissolution. In summary, the burst release of drugs from PCL/PEO nanofibers is primarily due to the hydrophilic nature of PEO, the large surface area of the nanofibers, the solubility of the drug, and the specific interactions between the polymers. These factors combine to enable rapid drug release from the surface and near-surface regions of the fibers. The release of gallic acid is more efficient compared to that of berberine chloride, which may be attributed to their differing solubilities. Gallic acid exhibits relatively good water solubility, enabling it to dissolve and be released more easily from formulations. In contrast, berberine chloride has lower water solubility, which can restrict its release rate.

Amelioration of psoriatic phenotypes by the SDF–PCL/PEO nanofibrous mesh in IMQ-induced mice

To evaluate the anti-psoriatic effects of SDF–PCL/PEO nanofibrous meshes *in vivo*, a formulation of PCL/PEO loaded with 0.2%, 1%, or 5% SDF was topically applied to the shaved back skin and ears of BALB/c mice for 30 min each day. This treatment was conducted alongside the application of imiquimod (IMQ) cream for seven consecutive days. Clobetasol propionate (CP) and SDF ointment were used as positive and comparative controls, respectively, while the mice were weighed daily throughout the experiment (Fig. 4A). Compared to the control group, the IMQ-treated model group exhibited typical psoriasis-like symptoms, such as erythema, scaling, and thickened skin/ear (Fig. 4B and C). When compared to IMQ-induced mice that did not receive drug treatment, the psoriatic skin treated with CP, SDF ointment, PCL/PEO, or SDF–PCL/PEO groups (0.2% SDF, 1% SDF, 5% SDF) displayed an overall improvement in skin erythema, scaling, and skin thickness by day 7, although the degree of improvement varied among treatments. Notably, weight loss resulting from IMQ treatment appeared to be partially restored (Fig. S1†), which correlated with the recovery of the psoriasis-like appearance of the skin and right ear in the experimental mice (Fig. S2 and S3†). The application of SDF ointment led to modest improvements in erythema, scaling, and skin thickness compared to IMQ model mice. However, the psoriatic skin lesions treated with SDF ointment were notably stained a dark brown color. As previously reported,[32] the PCL/PEO has anti-inflammatory properties that can alleviate the psoriasis-like symptoms to some degree. Notably, the severity of skin damage induced by IMQ was significantly reduced in mice treated with the SDF–PCL/PEO formulations. Consistent with the appearance of the skin and ears, the PASI scores, which evaluated erythema, scaling, and skin/ear thickness, demonstrated varying degrees of efficacy in drug-treated groups compared to IMQ group, as shown in Fig. 4D. Among different groups of SDF–PCL/PEO, mice treated with 5% SDF–PCL/PEO exhibited markedly lower PASI scores than those of the 0.2% and 1% SDF–PCL/PEO groups. Overall, our findings confirm that a daily 30-minute treatment with the SDF–PCL/PEO nanofibrous mesh is effective and superior to SDF ointment in alleviating psoriatic symptoms, with no signs of lesion discoloration.

Inhibition of psoriatic hyperplasia and inflammation, and angiogenesis by the SDF–PCL/PEO nanofibrous membrane in IMQ-induced mice

To gain a deeper understanding of the therapeutic efficacy of SDF–PCL/PEO on psoriatic alterations, pathological examinations were conducted and quantified (Fig. 5A and B). Initially, H&E staining effectively demonstrated the pattern of epidermal thickness regarding psoriatic hyperplasia (Fig. 5A), which revealed a 7-fold increase in thickness in IMQ-exposed skin compared to normal skin ($p < 0.0005$). Compared to the IMQ model, the SDF–PCL/PEO significantly reduced the thickness of epidermis in a dose-dependent manner, with 48.2 ± 2.23% in 0.2% SDF–PCL/PEO ($p < 0.0005$), 61.77 ± 4.21% in 1% SDF–PCL/PEO ($p < 0.0005$), and 71.21 ± 2.17% in 5% SDF–PCL/PEO ($p < 0.0005$). This thickening of the epidermis is associated with intense cell proliferation in the basal layer and irregular maturation of keratinocytes. Consequently, we quantified cell proliferation using Ki67, a nuclear protein present in proliferating cells within the epidermis, particularly in keratinocytes. As shown in Fig. 5A, there was a remarkable increase in Ki67 observed in the basal layer following IMQ treatment (indicated by green arrows in Fig. 5A), which correlated with the clinical severity of IMQ-induced psoriasis-like skin inflammation. Sparse Ki67 staining was noted in the SDF ointment and PCL/PEO groups. SDF ointment exhibited a reduction in $Ki67^+$ cells of 56.59 ± 3.61% ($p < 0.0005$). The SDF–PCL/PEO reduced the number of $Ki67^+$ cells in a dose-dependent manner, with 79.1 ± 2.27% in 0.2% SDF–PCL/PEO ($p < 0.0005$), 86.17 ± 1.64% in 1% SDF–PCL/PEO ($p < 0.0005$), and 90.68 ± 1.64% in 5% SDF–PCL/PEO ($p < 0.0005$) compared to the IMQ-induced untreated model. These data support the effective protective role of the

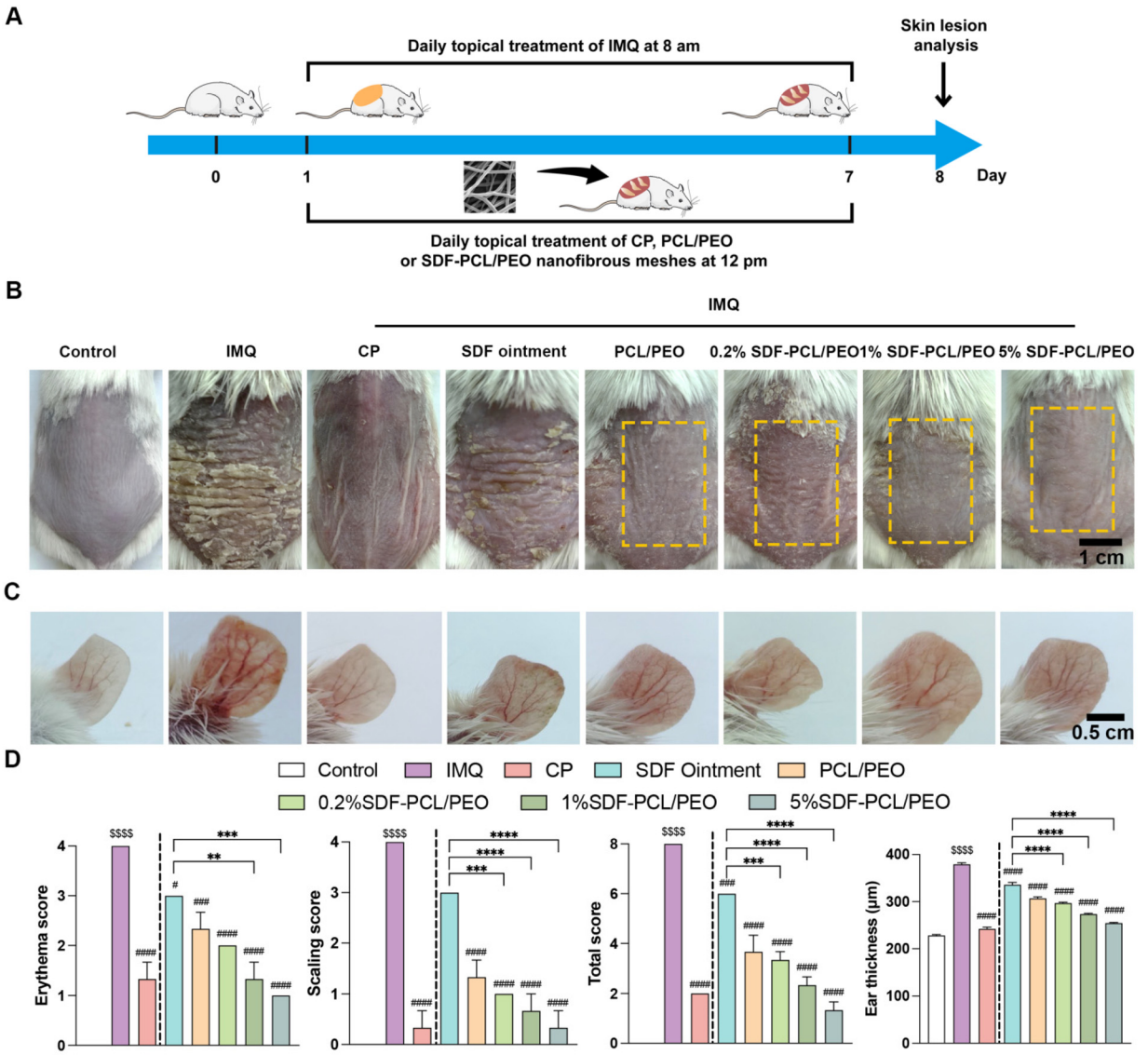

Fig. 4 Amelioration of psoriatic phenotypes by SDF nanofibrous meshes in IMQ-induced mice. (A) Experimental design used to assess the anti-psoriasis efficacy of SDF nanofibrous meshes in a mouse model with psoriasis-like symptoms induced by IMQ. (B) The macroscopic appearance of the dorsal shaved skin of mice treated with the indicated formulations, with CP as a positive control. The dashed yellow boxes indicate the site of mesh application. Scale bar: 1 cm. (C) Macroscopic appearance of the right ear of mice treated with the designated formulations. Scale bar: 0.5 cm. (D) Assessment of erythema, scaling, total PASI, and ear thickness of the IMQ-induced psoriatic dorsal skin of mice receiving the indicated treatments (n = 3). Data are presented as the mean ± SEM. $^{\$\$\$\$}p < 0.001$ compared to control; $^{\#}p < 0.05$, $^{\#\#\#}p < 0.005$, and $^{\#\#\#\#}p < 0.001$ compared to IMQ; $^{**}p < 0.01$, $^{***}p < 0.005$, and $^{****}p < 0.001$ between treatments as indicated.

SDF–PCL/PEO nanofibrous membrane against hyperproliferation in psoriatic skin. Additionally, in the context of inflammation in psoriatic tissues, macrophages emerged as the primary inflammatory cells involved. CD68, an immune cell marker for macrophages, plays a pivotal role in the chronic inflammatory process. By assessing CD68 levels, we observed a significant increase of 243.66 ± 17.21 ($p < 0.0005$) in resident dermal macrophages following IMQ exposure in lesional skin compared to normal skin (indicated by red arrows in Fig. 5A), suggesting that macrophages were activated and recruited to the lesioned plaque. In contrast, in the application to mouse groups of the topical SDF ointment, PCL/PEO and varying concentrations of SDF–PCL/PEO the inflammatory infiltrates were effectively reduced. Among all treated groups, mice treated with 5% SDF–PCL/PEO showed the most significant reduction of 76.64 ± 3.41 ($p < 0.0005$) in the mean population of $CD68^{+}$ cells. Furthermore, alongside keratinocyte proliferation and inflammation, angiogenesis plays a significant role in the pathogenesis of psoriasis.[39–41] As revealed through the examination of full-thickness grafts in response to IMQ, the lesioned skin of mice displayed significantly dilated and convoluted blood vessels, which are associated with angiogenesis, when stained

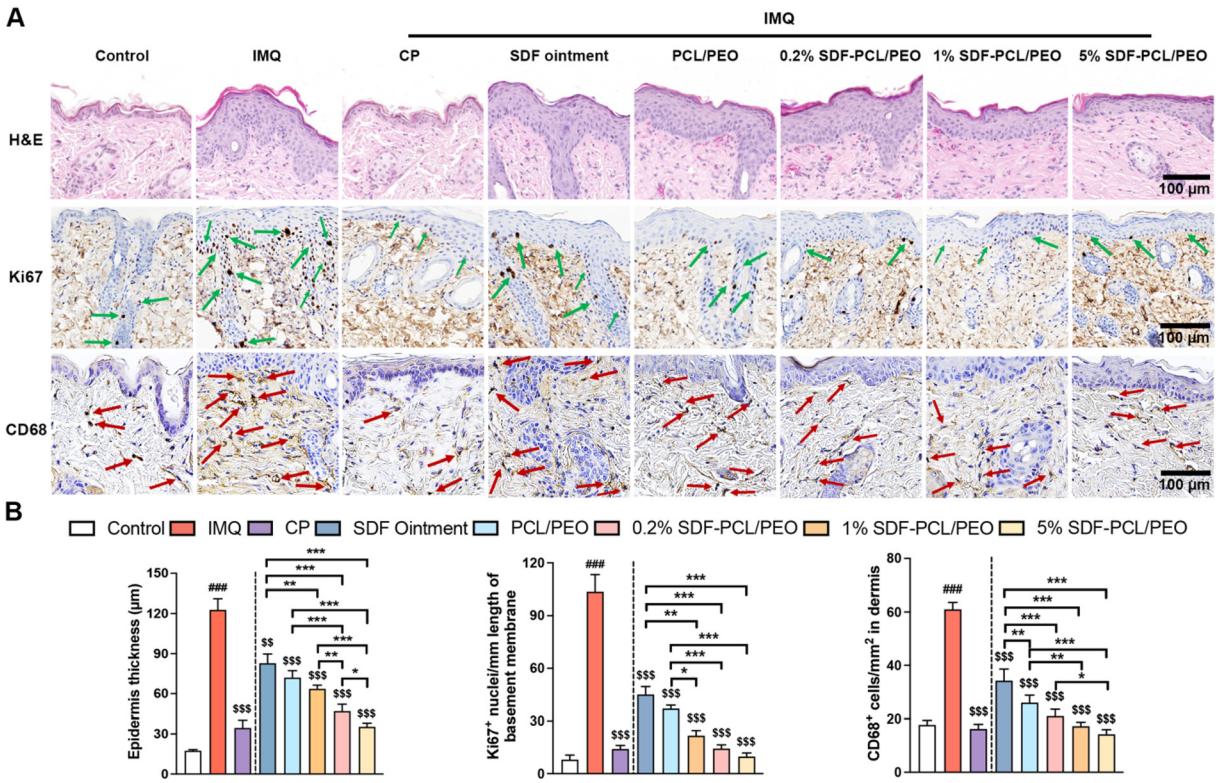

Fig. 5 Pathological analyses of the dorsal skin in response to SDF nanofibrous meshes in IMQ-induced psoriasis. (A) H&E staining, expression level of Ki67 (green arrow) and CD68 (red arrow) in the dorsal skin of psoriatic mice treated with the indicated formulations. Scale bar: 100 μm. (B) Quantitative analyses of (A) in terms of epidermal thickness, Ki67-positive cells, and CD68-labelled cells. Data are presented as the mean ± SEM. $^{###}p < 0.005$ compared to control; $^{\$}p < 0.05$, $^{\$\$}p < 0.01$, and $^{\$\$\$}p < 0.005$ compared to IMQ; $^{*}p < 0.05$, $^{**}p < 0.01$, and $^{***}p < 0.005$ between treatments as indicated.

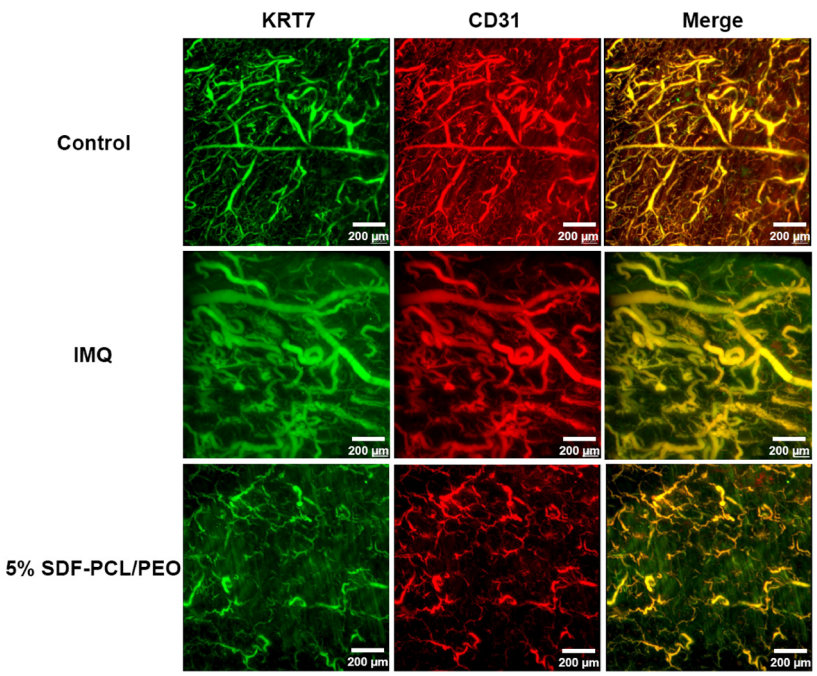

Fig. 6 The effect of the SDF–PCL/PEO nanofibrous mesh on vascular morphology in IMQ-induced mice. Full-thickness skin grafts were harvested from the control, IMQ, and 5% SDF–PCL/PEO nanofiber mesh groups. For deep-tissue imaging, grafts were subjected to optical clearing techniques using optical clearing agents and immunostained with the epithelial marker KRT7 (green) and the vascular marker CD31 (red). Scale bar: 200 μm.

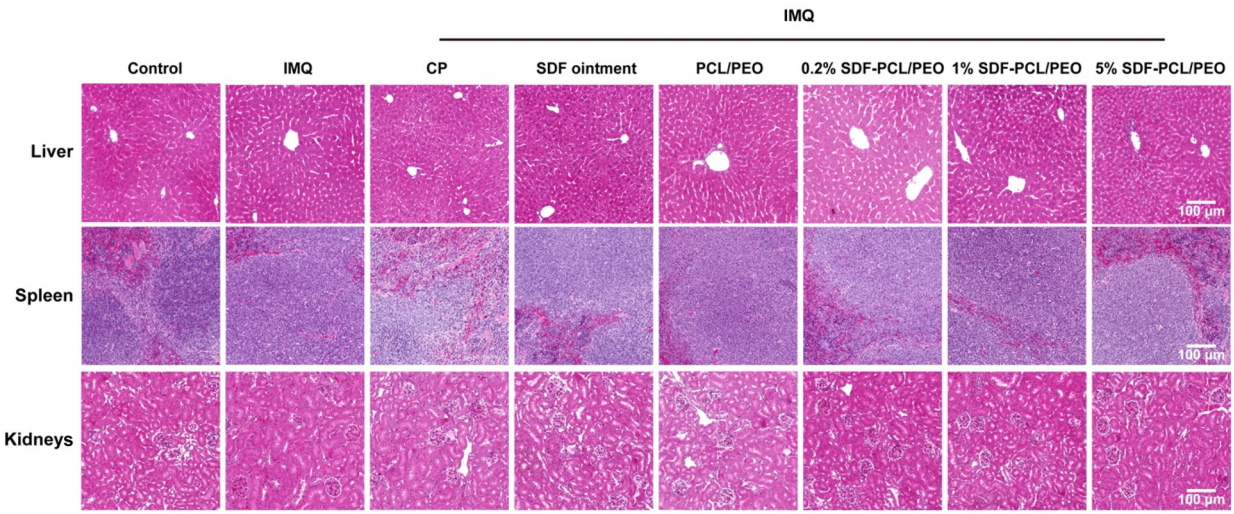

Fig. 7 Safety evaluation of nanofibrous meshes *in vivo* in psoriatic mice. Representative images showing H&E staining of sections of liver (top panels), spleen (middle panels), and kidneys (bottom panels) from the experimental mice. Scale bar: 100 μm.

with CD31 (Fig. 6). Due to substantial experimental costs associated with the staining of full-thickness skin grafts, we prioritized the evaluation of the SDF–PCL/PEO at 5% to address the anti-angiogenesis capability of SDF–PCL/PEO. The provision of SDF nanofibrous membrane effectively normalized the development of dilated and tortuous blood vessels, verifying the therapeutic efficacy of SDF–PCL/PEO. Additionally, the safety profile of SDF–PCL/PEO was validated through pathological examinations of the liver, kidneys, and spleen (Fig. 7). Histopathological analysis demonstrated that the hepatic cords in each group were well-organized, radiating from the central vein towards the surrounding areas. The majority of hepatocytes appeared intact, showing no evidence of punctate necrosis or inflammatory cell infiltration. Alterations in both the red and white pulp of the spleen were consistent with splenomegaly caused by imiquimod (IMQ). The kidney cells were regularly and orderly arranged, with the morphological structures of the glomeruli and renal interstitium remaining normal. No inflammatory exudate or connective tissue hyperplasia was noted. These findings suggest that the topical application of SDF–PCL/PEO did not exhibit any histopathological toxicity *in vivo*. Collectively, this set of data demonstrated the overall anti-IMQ-induced psoriasis-like skin inflammation efficacy of SDF in an IMQ-induced psoriasis model, highlighting the benefits of the SDF–PCL/PEO nanofibrous membrane.

Conclusions

The use of nanoparticles and liposomes for the delivery of bioactive components from Chinese medicine has been explored.[42] However, challenges persist in achieving efficient drug loading and effectively encapsulating and delivering these complex mixtures while preserving their therapeutic properties. This study employed electrospinning technology to transform the conventionally used SDF ointment into nanofibrous meshes, which offer improved bioavailability, stability, mechanical properties, and increased surface area for drug loading. This innovation leads to more efficient drug component delivery to affected skin areas, maximizing synergistic effects while minimizing staining issues, which reduces the frequency of application and enhances patient compliance. The resulting electrospun fibrous membranes exhibit a continuous, smooth structure free of beads, showcasing excellent amphiphilic properties. Five components of the SDF, including *Phellodendron chinense*, *Indigo naturalis*, *Gallae chinensis*, Gypsum fibrosum, and calamine, were identified in the SDF–PCL/PEO membrane. Additionally, berberine chloride from *Phellodendron chinense* and gallic acid from *Gallae chinensis* were successfully released from the SDF–PCL/PEO nanofibrous membrane. Functionally, the SDF–PCL/PEO nanofibrous membrane demonstrated significant effectiveness in alleviating psoriatic symptoms without noticeable adverse alterations. Due to the unique features of electrospun nanofibers, the SDF membranes require only 30 min of application and do not leave stains, in contrast to the traditional SDF ointment. This study presents a viable strategy for transforming complex natural products into effective external therapies for IMQ-induced psoriasis-like skin inflammation, offering a promising solution for individuals seeking relief. Future research should concentrate on further optimizing the formulation and processing conditions, exploring their clinical potential, and addressing any safety concerns that may arise.

The integration of SDF into nanofibers for the treatment of IMQ-induced psoriasis-like skin inflammation offers a promising and innovative strategy that presents several advantages, including targeted delivery, improved bioavailability, and sustained release of active ingredients. However, despite these notable advancements, several limitations must be recognized and should be addressed in future research. First, variations in the source materials, extraction methods, and processing con-

ditions can lead to inconsistencies in the final product. Second, while the biocompatibility of SDF nanofibers is generally favorable, it is essential to conduct thorough investigations into any potential adverse reactions across diverse patient populations. Lastly, the high cost associated with nanofiber development may limit accessibility. In conclusion, while the incorporation of SDF into nanofibers for IMQ-induced psoriasis-like skin inflammation therapy holds great promise, it is vital to tackle the limitations related to standardization, biocompatibility, scalability, and patient acceptance. By addressing these issues, this innovative approach has the potential to revolutionize psoriasis treatment, providing a more effective and personalized therapeutic strategy.

Author contributions

All authors have contributed to the preparation of this manuscript and have approved its submission for publication.

Conflicts of interest

The authors declare no conflict of interest related to this article.

Data availability

All data generated or analyzed during this study are included in this published article and its ESI.†

Acknowledgements

We gratefully acknowledge the funding from the Beijing Traditional Chinese Medicine Technology Development Foundation (BJZYYB-2023-18), Beijing Dongcheng Talent Development Foundation (2024-dchrcpyzz-44), Fundamental Research Funds for the Central Public Welfare Research Institutes (YZX-202412, YPX-202301), and the TCM Theory Inheritance and Innovation Project of CACMS Innovation Fund (KYG-202405). The authors thank Prof. Zhenji Li from the World Federation of Chinese Medicine Societies for his support and valuable input.

References

1 R. Parisi, *et al.*, National, regional, and worldwide epidemiology of psoriasis: systematic analysis and modelling study, *Br. Med. J.*, 2020, **369**, m1590.
2 D. J. Veale and U. Fearon, The pathogenesis of psoriatic arthritis, *Lancet*, 2018, **391**(10136), 2273–2284.
3 A. W. Armstrong and C. Read, Pathophysiology, Clinical Presentation, and Treatment of Psoriasis: A Review, *J. Am. Med. Assoc.*, 2020, **323**(19), 1945–1960.
4 W.-H. Boehncke and M. P. Schön, Psoriasis, *Lancet*, 2015, **386**(9997), 983–994.
5 S. P. Raychaudhuri, *et al.*, Management of psoriatic arthritis: Early diagnosis, monitoring of disease severity and cutting edge therapies, *J. Autoimmun.*, 2017, **76**, 21–37.
6 M. Anheyer, *et al.*, Herbal medicine for treating psoriasis: A systematic review, *Complement Ther. Med.*, 2025, **90**, 103173.
7 Y. Luo, *et al.*, Chinese Herbal Medicine for Psoriasis: Evidence From 11 High-Quality Randomized Controlled Trials, *Front. Pharmacol.*, 2020, **11**, 599433.
8 Y. Yan, *et al.*, Exploratory clinical trial to evaluate the efficacy of a topical traditional chinese herbal medicine in psoriasis vulgaris, *J. Evidence-Based Complementary Altern. Med.*, 2015, 719641.
9 K. Dhiman, A. Sharma, K. Goyal, V. Pandit, M. S. Ashawat and S. Jindal, Application of Berberin on Skin Diseases: A Review, *Research Journal of Pharmaceutical Dosage Forms and Technology*, 2022, **14**(4), 4.
10 J. Bai, *et al.*, Gallic acid: Pharmacological activities and molecular mechanisms involved in inflammation-related diseases, *Biomed. Pharmacother.*, 2021, **133**, 110985.
11 Y. Qi-yue, *et al.*, From natural dye to herbal medicine: a systematic review of chemical constituents, pharmacological effects and clinical applications of indigo naturalis, *Chin. Med.*, 2020, **15**(1), 127.
12 A. Phogat, J. Singh and V. Malik, Pharmacological effects of Berberine – A Chinese medicine, against xenobiotics toxicity, *Pharmacol. Res. – Mod. Chin. Med.*, 2024, **13**, 100507.
13 S. Gu, *et al.*, Clinical, pharmacology and in vivo studies of QingDai (indigo naturalis) promotes mucosal healing and symptom improvement in ulcerative colitis by regulating the AHR-Th17/Treg pathway, *J. Inflammation*, 2024, **21(1)**, 44.
14 M. Singhal, M. Lapteva and Y. N. Kalia, Formulation challenges for 21st century topical and transdermal delivery systems, *Expert Opin. Drug Delivery*, 2017, **14**(6), 705–708.
15 A. R. Yadav, *et al.*, Challenges in Formulating Transdermal Systems for Treating Chronic Skin Infections, *Curr. Opin. Pharmacol.*, 2025, 102540.
16 V. Vijaykumar, M. Saikiran, V. R. Bharathy and U. Ubaidulla, Formulation Challenges in Dermal Drug Delivery Systems: A Comprehensive Review of Physicochemical Properties and Advanced Delivery Strategies, *Int. J. Drug Deliv. Technol.*, 2024, **14**, 1124–1129.
17 Y. Bao, S. Z and W. Shi, Percutaneous absorption effects of Chinese herbal medicine, *Afr. J. Pharm. Pharmacol.*, 2012, **6**(6), 7.
18 Y. B. Zhang, *et al.*, Nano-based drug delivery systems for active ingredients from traditional Chinese medicine: Harnessing the power of nanotechnology, *Front. Pharmacol.*, 2024, **15**, 1405252.
19 N. Raina, *et al.*, New Insights in Topical Drug Delivery for Skin Disorders: From a Nanotechnological Perspective, *ACS Omega*, 2023, **8**(22), 19145–19167.
20 H.-Y. Chiu and T.-F. Tsai, Topical use of systemic drugs in dermatology: A comprehensive review, *J. Am. Acad. Dermatol.*, 2011, **65**(5), 1048.e1–1048.e22.

21 Y. Cho, *et al.*, Electrospinning and Nanofiber Technology: Fundamentals, Innovations, and Applications, *Adv. Mater.*, 2025, e2500162.
22 A. Luraghi, F. Peri and L. Moroni, Electrospinning for drug delivery applications: A review, *J. Controlled Release*, 2021, **334**, 463–484.
23 D. Ji, *et al.*, Electrospinning of nanofibres, *Nat. Rev. Methods Primers*, 2024, **4**(1), 1.
24 J. Xue, *et al.*, Electrospinning and Electrospun Nanofibers: Methods, Materials, and Applications, *Chem. Rev.*, 2019, **119**(8), 5298–5415.
25 X. Feng, *et al.*, Electrospun polymer micro/nanofibers as pharmaceutical repositories for healthcare, *J. Controlled Release*, 2019, **302**, 19–41.
26 T. C. Mokhena, *et al.*, Electrospun PCL-Based Materials for Health-Care Applications: An Overview, *Macromol. Mater. Eng.*, 2024, **309**(8), 2300388.
27 A. Azari, *et al.*, Electrospun Polycaprolactone Nanofibers: Current Research and Applications in Biomedical Application, *Adv. Pharm. Bull.*, 2021, **12**, 658–672.
28 X. Y. D. Soo, *et al.*, Electrospun PEO/PEG fibers as potential flexible phase change materials for thermal energy regulation, *Exploration*, 2024, **4**(1), 20230016.
29 R. Xu, *et al.*, Janus double-sided nanofibrous patch with asymmetric wettability and controlled topical delivery of tryptanthrin and indirubin as an effective therapy for psoriasis, *Mater. Today Bio*, 2025, **32**, 101822.
30 S. Guo, *et al.*, Transformation of Natural Resin Resina Draconis to 3D Functionalized Fibrous Scaffolds for Efficient Chronic Wound Healing, *Adv. Healthc. Mater.*, 2024, **13**(30), e2401105.
31 V. Kupka, *et al.*, Well-Blended PCL/PEO Electrospun Nanofibers with Functional Properties Enhanced by Plasma Processing, *Polymers*, 2020, **12**(6), 1403.
32 P. Wang, *et al.*, Benefits of topical indigo naturalis nanofibrous patch on psoriatic skin: A transdermal strategy for botanicals, *Mater. Today Bio*, 2023, **22**, 100756.
33 R.-z. Tan, *et al.*, Macrophages mediate psoriasis via Mincle-dependent mechanism in mice, *Cell Death Discovery*, 2023, **9**(1), 140.
34 A. Nadeem, *et al.*, Imiquimod-induced psoriasis-like skin inflammation is suppressed by BET bromodomain inhibitor in mice through RORC/IL-17A pathway modulation, *Pharmacol. Res.*, 2015, **99**, 248–257.
35 D.-h. Wu, *et al.*, PSORI-CM02 alleviates IMQ-induced mouse dermatitis via differentially regulating pro- and anti-inflammatory cytokines targeting of Th2 specific transcript factor GATA3, *Biomed. Pharmacother.*, 2019, **110**, 265–274.
36 J. R. Dias, P. L. Granja and P. J. Bartolo, Advances in electrospun skin substitutes, *Prog. Mater. Sci.*, 2016, **84**, 314–334.
37 R. Punyamurthy, *et al.*, Abaca Fiber Reinforced Hybrid Composites, *Int. J. Appl. Eng. Res.*, 2014, **9**, 20273–20286.
38 S. F. Chou and K. A. Woodrow, Relationships between mechanical properties and drug release from electrospun fibers of PCL and PLGA blends, *J. Mech. Behav. Biomed. Mater.*, 2017, **65**, 724–733.
39 X. Zhou, *et al.*, Advances in the pathogenesis of psoriasis: from keratinocyte perspective, *Cell Death Dis.*, 2022, **13**(1), 81.
40 R. Heidenreich, M. Rocken and K. Ghoreschi, Angiogenesis drives psoriasis pathogenesis, *Int. J. Exp. Pathol.*, 2009, **90**(3), 232–248.
41 D. Creamer, *et al.*, Angiogenesis in psoriasis, *Angiogenesis*, 2002, **5**(4), 231–236.
42 P. Wang, *et al.*, Ethosomes-mediated tryptanthrin delivery as efficient anti-psoriatic nanotherapy by enhancing topical drug absorption and lipid homeostasis, *J. Nanobiotechnol.*, 2024, **22**(1), 584.